

Quantum Thermal Machine as a Thermometer

Patrick P. Hofer,^{1,*} Jonatan Bohr Brask,¹ Martí Perarnau-Llobet,^{2,3} and Nicolas Brunner¹

¹Group of Applied Physics, University of Geneva, Switzerland

²Max-Planck-Institut für Quantenoptik, Hans-Kopfermann-Str. 1, D-85748 Garching, Germany

³ICFO-Institut de Ciències Fotoniques, The Barcelona Institute of Science and Technology, 08860 Castelldefels, Barcelona, Spain

(Dated: June 18, 2022)

We propose the use of a quantum thermal machine for low-temperature thermometry. A hot thermal reservoir coupled to the machine allows for simultaneously cooling the sample while determining its temperature without knowing the model-dependent coupling constants. In its most simple form, the proposed scheme works for all thermal machines which perform at Otto efficiency and can reach Carnot efficiency. We consider a circuit QED implementation which allows for precise thermometry down to ~ 15 mK with realistic parameters. Based on the quantum Fisher information, this is close to the optimal achievable performance.

Introduction.— Accurate sensing and measuring of temperature is of crucial importance throughout natural science and technology. Increased capabilities of control and imaging on smaller and smaller scales have led to the need for precise thermometry down to millikelvin temperatures at sub-micron scales. Conventional techniques are not applicable in this regime, resulting in the development of a broad range of new methods over the last decade [1]. Many of these employ probes which are so small that quantum effects become relevant in their design and sensing capabilities, e.g. quantum dots [2–4], nitrogen-vacancy centers in diamond [5–7], superconducting quantum interference devices [8], and even biomolecules [9]. At the same time, the study of thermal processes in the quantum regime has recently seen increased interest fueled by tools developed in quantum information theory [10, 11]. This approach has led to novel insights into the limitations of measuring cold temperatures posed by quantum theory [12–14], showing that coherence can be beneficial for low temperature thermometry [12, 15–18].

In a standard approach to thermometry, a probe is brought into thermal contact with the sample and the system is allowed to equilibrate [3, 4]. The temperature is then read out through some observable on the probe whose relation to the temperature is known. The measurement can possibly be improved by letting the probe interact with the sample for a finite time only, making use of the transient dynamics [15, 19], or by increasing the coupling strength between sample and probe [20]. Both of these approaches lead to a non-equilibrium state for the probe. Another approach to thermometry, which is employed to measure electronic temperatures, makes use of a voltage bias that creates an out-of-equilibrium situation. The temperature can then be determined through the current-voltage characteristics [21, 22]. We note that these strategies generally lead to unwanted heating of the sample.

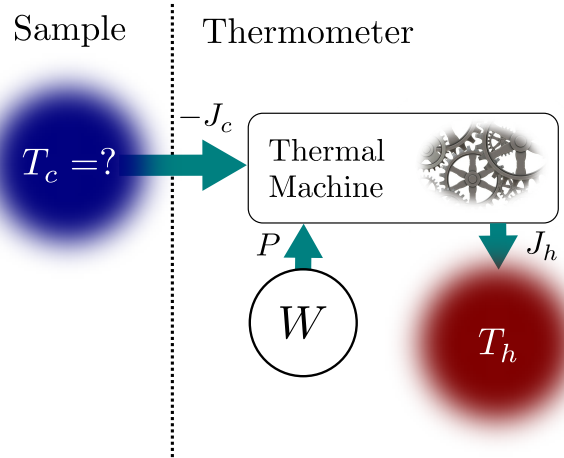


FIG. 1. Sketch of the thermometer. In order to measure the temperature of the cold bath, a quantum thermal machine is operated as a refrigerator, inducing a heat current from the cold bath to the hot bath. This requires energy from the work source W . The hot temperature is then increased until the machine reaches the Carnot point where its power consumption and the heat flows vanish (i.e. $P = J_c = J_h = 0$). For machines that perform with a well known efficiency (e.g. the Otto efficiency $\eta = 1 - \Omega_c/\Omega_h$), the cold temperature can then be deduced from the hot temperature through the relation $\eta = \eta_C = 1 - T_c/T_h$, without the need of knowing any model-dependent coupling constants. In this way, a low precision measurement of a hot temperature is converted into a high precision measurement of a low temperature. Operating the thermal machine as a refrigerator avoids any heating of the cold bath.

In this letter, we connect thermometry to quantum thermal machines. Such machines are extensively studied to investigate fundamental as well as practical aspects of quantum thermodynamics [10, 23–25]. By construction, these machines constitute out-of-equilibrium systems including a temperature gradient. Here we consider a quantum refrigerator to simultaneously cool the sample and estimate its temperature. This way, the proposed thermometer does not induce any heating of the sample, even

* patrick.hofer@unige.ch

if it is at the coldest temperature that is experimentally available. To the best of our knowledge, our proposal is the first to make use of a *thermal* bias to obtain an out-of-equilibrium situation that is favorable for thermometry. Note that albeit the thermal bias, the sample is assumed to remain in *local* equilibrium throughout the measurement.

The main idea is illustrated in Fig. 1. The sample to be measured is a thermal bath at a cold temperature T_c . Through a small quantum system (the machine), the sample is coupled to another bath at a higher temperature T_h and an external power source (which in principle could be provided by a third thermal bath [26–29]). Note that this setup can operate either as a refrigerator, with the power source driving a heat flow from the cold to the hot bath, or as a heat engine, where work is generated using a heat flow from the hot to the cold bath [23, 30–35]. Since we are interested in determining T_c , the whole setup, apart from the cold bath, should be considered as the thermometer. By operating the machine as a refrigerator, the sample will be cooled during the measurement of T_c , avoiding any undesirable heating. Furthermore, by approaching the Carnot point, where the machine approaches reversibility, the need for knowledge of the coupling constants can be eliminated, just as for thermalizing thermometry. We note that some knowledge of the hot bath temperature is required for our scheme. However, the cold temperature can be determined with high precision even if the hot temperature measurement is noisy. Our scheme can thus be seen as a method to turn an uncertain measurement of warm temperatures into precise measurements of cold temperatures [36].

The rest of this letter is structured as follows. After describing the working principle of the proposed thermometer in more detail, we discuss an implementation in a circuit QED architecture, which allows for precise thermometry down to ~ 15 mK using realistic parameters. Finally, we investigate the precision of the thermometer using the quantum Fisher information.

Scheme.— We now turn to a more detailed description of our thermometer. The thermal bias and the power source induce energy flows denoted by J_c (heat flow into the cold bath), J_h (heat flow into the hot bath), and P (power consumption, see Fig. 1). The power consumed by the machine will in general be a function of the temperatures as well as the model-dependent parameters. Inverting this relationship, the cold temperature will have a functional dependence

$$T_c = f(P, T_h). \quad (1)$$

Here, f might have a complicated dependence on the cou-

$\Omega_h/2\pi$	$\Omega_c/2\pi$	$\kappa/2\pi$	$E_J/2\pi$	λ	ΔI	ΔT_h
8.5 GHz	1 GHz	0.06 GHz	0.2 GHz	0.3	0.3 pA	10 mK

TABLE I. Realistic Parameters for operating the proposed thermometer. Here $\kappa = \kappa_h = \kappa_c$ and $\lambda = \lambda_h = \lambda_c$.

pling constants or any other model dependent parameters. However, the relation simplifies for machines that perform at the Otto efficiency and exhibit a Carnot point [38]. When the machine is operated as a heat engine, the efficiency is defined as $\eta = P/J_h$. The Otto efficiency is given by $\eta = 1 - \Omega_c/\Omega_h$ where Ω_c, Ω_h are frequencies that depend on the architecture of the machine (see Fig. 2). For thermal machines that exhibit a Carnot point, setting the frequencies and temperatures such that

$$\eta = 1 - \frac{\Omega_c}{\Omega_h} = 1 - \frac{T_c}{T_h} = \eta_C, \quad (2)$$

results in vanishing energy flows. Examples of thermal machines which operate at the Otto efficiency and exhibit a Carnot point are discussed in Refs. [24, 39–44]. We note that whenever the frequencies and temperatures are such that $\eta > \eta_C$, the machine operates as a refrigerator. At the Carnot point, we find the simple relation

$$T_c = \frac{\Omega_c}{\Omega_h} T_h, \quad (3)$$

implying that $f(P=0, T_h) = T_h \Omega_c/\Omega_h$ is independent of any coupling constants. The cold temperature can then be determined using the following strategy (see Fig. 3)

1. Initiate the machine to act as a refrigerator, i.e. $T_h < T_c \Omega_h/\Omega_c$, and monitor P
2. Increase T_h until $P = 0$ is reached
3. Measure T_h
4. Determine T_c using Eq. (3)

Our scheme thus relies on a hot bath $T_h > T_c$ with a tunable temperature. Two quantities are measured to determine T_c : The power consumption P and the hot

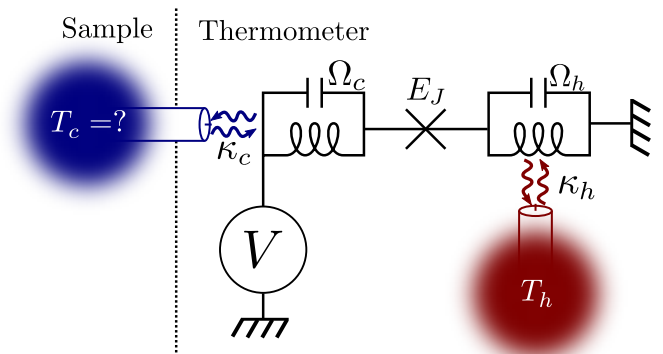


FIG. 2. Circuit QED implementation of the thermometer. Two harmonic oscillators with frequencies Ω_h and Ω_c are coupled to thermal baths at temperatures T_c and T_h respectively and to each other through a Josephson junction. The external bias voltage V ensures that the cold bath is being cooled while determining T_c .

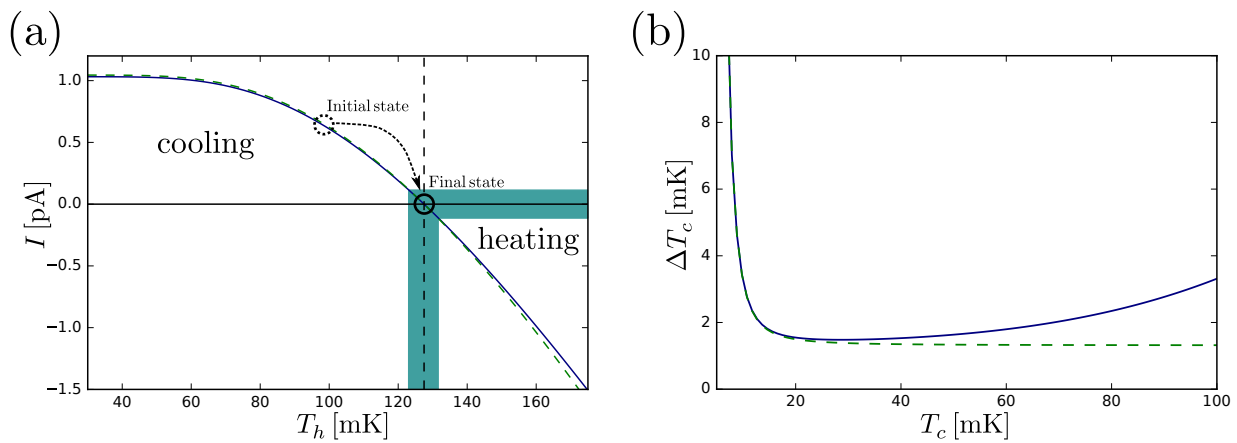


FIG. 3. Performance of a circuit QED implementation. (a) Charge current as a function of the hot temperature T_h for fixed $T_c = 15$ mK. The refrigerator is initiated at T_h below the Carnot point (dotted circle) leading to cooling of the cold bath. T_h is then increased until the current vanishes (solid circle). This point can only be determined up to a certain error ΔI which induces an uncertainty in the final T_h (shaded area) reducing the accuracy of the measurement of T_c . The bigger $|\partial_{T_h} I|$, the smaller the induced error. (b) Error in the temperature estimation. Two sources of error limit the accuracy of measuring T_c . The Carnot point can only approximately be reached due to a finite resolution in the current measurement ΔI [see panel (a)] and the hot temperature can only be measured with an accuracy ΔT_h . The total resulting error ΔT_c is given in Eq. (4) and plotted as a function of T_c . Measurement errors of $\Delta I = 0.3$ pA and $\Delta T_h = 10$ mK lead to $\Delta T_c < 2$ mK down to temperatures of 15 mK. Blue (solid) lines are numeric solutions, green (dashed) lines are obtained analytically using a simplified model [37].

temperature T_h . Both of these measurements are accompanied by errors, ΔP and ΔT_h . Simple error propagation yields (assuming independent errors)

$$\Delta T_c = \sqrt{\left(\frac{\partial f}{\partial P}\right)^2 (\Delta P)^2 + \left(\frac{\partial f}{\partial T_h}\right)^2 (\Delta T_h)^2}. \quad (4)$$

The error thus depends on the derivatives of f which generally depend on model-specific parameters. Note however that $\partial_{T_h} f|_{P=0} = \Omega_c/\Omega_h$ implying that the error induced by the measurement of T_h only depends on the frequencies. Any uncertainty in the measurement of T_h can thus be compensated by increasing the ratio Ω_h/Ω_c and thus does not represent a fundamental limit.

Circuit QED implementation.— We now turn to an implementation of these ideas, considering the heat engine proposed in Ref. [43] and sketched in Fig. 2. In this machine, the quantum system consists of two LC -oscillators coupled to each other through a Josephson junction. Each oscillator is coupled individually to a heat bath, and the power source is provided by an external voltage bias. We note that a similar setup (without any temperature bias however) has been considered for thermometry in Ref. [45]. The Hamiltonian describing the system reads (in a rotating frame)

$$\hat{H} = \frac{E_J}{2} \left(\hat{a}_h^\dagger \hat{A}_h \hat{A}_c \hat{a}_c + H.c. \right), \quad (5)$$

where E_J is the Josephson energy and the non-linear operators \hat{A}_α are defined as

$$\hat{A}_\alpha = 2\lambda_\alpha e^{-2\lambda_\alpha^2} \sum_{n_\alpha=0}^{\infty} \frac{L_{n_\alpha}^{(1)}(4\lambda_\alpha^2)}{n_\alpha + 1} |n_\alpha\rangle \langle n_\alpha|, \quad (6)$$

with $L_n^{(k)}(x)$ denoting the generalized Laguerre polynomials and $|n_\alpha\rangle$ Fock states. We note that Eq. (5) is derived using a rotating wave approximation which holds under the resonance condition

$$2eV = \Omega_h - \Omega_c, \quad (7)$$

where V is the external voltage and Ω_α is the frequency of the oscillator corresponding to the operator \hat{a}_α . The evolution of the system in contact with the thermal baths is captured by a local Lindblad master equation

$$\begin{aligned} \partial_t \hat{\rho} = & -i[\hat{H}, \hat{\rho}] + \kappa_h (n_B^h + 1) \mathcal{D}[\hat{a}_h] \hat{\rho} + \kappa_h n_B^h \mathcal{D}[\hat{a}_h^\dagger] \hat{\rho} \\ & + \kappa_c (n_B^c + 1) \mathcal{D}[\hat{a}_c] \hat{\rho} + \kappa_c n_B^c \mathcal{D}[\hat{a}_c^\dagger] \hat{\rho}, \end{aligned} \quad (8)$$

where we defined $\mathcal{D}[\hat{A}] \hat{\rho} = \hat{A} \hat{\rho} \hat{A}^\dagger - \{\hat{A}^\dagger \hat{A}, \hat{\rho}\}/2$, κ_α denotes the energy damping rate associated with the bath α , and $n_B^\alpha = [\exp(\frac{\Omega_\alpha}{k_B T_\alpha}) - 1]^{-1}$ the corresponding occupation number.

The power consumption of the machine is $P = IV$, where $I = \langle \hat{I} \rangle$ is the (dc) electrical current with the current operator

$$\hat{I} = -\frac{I_c}{2i} \left(\hat{a}_c^\dagger \hat{A}_c \hat{A}_h \hat{a}_h - H.c. \right), \quad (9)$$

and $I_c = 2eE_J$ the critical current. The mean heat currents are defined as

$$J_\alpha = \Omega_\alpha \kappa_\alpha (\langle \hat{n}_\alpha \rangle - n_B^\alpha). \quad (10)$$

As discussed in Ref. [43], this machine does perform at the Otto efficiency and can reach the Carnot efficiency

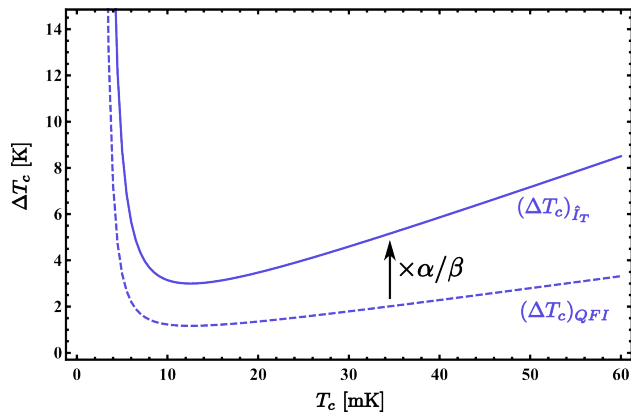


FIG. 4. Single-shot precision from a current measurement (blue solid) and from the QFI (blue dashed) at the Carnot point, for the simple model with oscillator frequencies and couplings given in Tab. I, and fitting parameter $g = E_J/8$.

at vanishing power. Furthermore, a tunable hot temperature could be implemented by heating one of the LC -oscillators using a microwave antenna.

Fig. 3(a) shows the electrical current as a function of the hot temperature and sketches the scheme for measuring T_c . The error of the measurement is plotted in Fig. 3(b), where the parameters (including the uncertainties) are given in Tab. I. We find a precision of $\Delta T_c \lesssim 2$ mK for temperatures down to $T_c \sim 15$ mK. Furthermore, in accordance with Ref. [43], we find good quantitative agreement with an approximate model obtained from Eq. (5) by replacing the non-linear operators \hat{A}_α by constants times the identity [37]. This model can be solved analytically and is used below to estimate the performance of our scheme using the quantum Fisher information.

Quantum Fisher information.— As already mentioned, the measurement error resulting from the hot temperature measurement is not of a fundamental nature since we can in principle reduce it by increasing Ω_h/Ω_c (note however that this implies an increase of T_h at the Carnot point). In order to understand how well the current measurement is doing in terms of temperature estimation, we turn to the quantum Fisher information.

The steady-state solution of Eq. (8) defines a family of states as a function of T_c (as well as all the other parameters in the setup). The quantum Fisher information (QFI) w.r.t T_c is a measure of the sensitivity of the state to changes in this parameter [46]. Through the quantum Cramer-Rao bound, it provides a lower bound on the mean-squared error in estimating T_c from any possible measurement [47]. Specifically, for a state ρ

$$(\Delta T_c)^2 \geq \frac{1}{\nu F(\rho)} \equiv \frac{1}{\nu} (\Delta T_c)_{QFI}^2, \quad (11)$$

where F is the QFI w.r.t. T_c and ν is the number of independent repetitions of the experiment. The bound is relevant (and can be saturated) in the local estimation

regime, where the prior on the estimated parameter is narrow and many repetitions are performed. In the same regime, for measuring a specific observable \hat{O} , the attainable precision is given by the error propagation formula

$$(\Delta T_c)^2 = \frac{(\Delta \hat{O})_\rho^2}{\nu |\partial_{T_c} \langle \hat{O} \rangle_\rho|^2} \equiv \frac{1}{\nu} (\Delta T_c)_{\hat{O}}^2. \quad (12)$$

Hence, by substituting the current operator for \hat{O} and comparing $(\Delta T_c)_{QFI}$ and $(\Delta T_c)_I$ evaluated in the steady state at the Carnot point, we can get an idea of how close the current measurement is to being optimal. Note that this neglects any errors in other parameters as well as the fact that our strategy is based on continuous measurements rather than projective measurements considered in Eq. (12). Although we should thus not expect this calculation to give us the actual uncertainty obtained in an experiment, it does tell us whether the current is a good choice of observable for estimating T_c .

To perform the comparison, we first need to find the steady-state solution of Eq. (8). This can be done analytically for the approximate model discussed in the supplemental information [37] yielding

$$(\Delta T_c)_{I_T} = \alpha \frac{T_c^2}{\Omega_c} \sinh\left(\frac{\Omega_c}{2T_c}\right), \quad (13)$$

and

$$(\Delta T_c)_{QFI} = \beta \frac{T_c^2}{\Omega_c} \sinh\left(\frac{\Omega_c}{2T_c}\right), \quad (14)$$

where the parameters α and β depend on the coupling constants and are given in the supplemental information [37]. We see that the current-measurement precision and the optimal precision from the QFI have exactly the same functional behavior with temperature and energy, but depend differently on the coupling constants. For any choice of couplings, $\alpha \geq \beta$ such that $(\Delta T_c)_{I_T} \geq (\Delta T_c)_{QFI}$. Both expressions are plotted in Fig. 4.

The smallest possible value of α is $4\sqrt{2}$, attained for $\kappa_c = \kappa_h = 2g$ (where g is the interaction strength in the approximate model). For the parameters in Tab. I, $\alpha/4\sqrt{2} \approx 1.02$, and so the current measurement is close to its best performance in this regime. Furthermore, $\alpha/\beta \approx 2.55$, hence it is also not far from the optimal precision obtainable by any possible measurement. The smallest possible value of α/β is $\sqrt{2 + \sqrt{2}} \approx 1.85$, however it is attained in the weak coupling limit $\kappa_c \rightarrow 0$, where no information about T_c can be extracted and both α and β diverge. In the opposite limit where the hot reservoir is disconnected, $\kappa_h \rightarrow 0$, we have $\alpha \rightarrow \infty$ while $\beta \rightarrow \sqrt{2}$ reaches its minimal value. This reflects the fact that the current vanishes if the system is coupled to a single bath only, while even if there is no coupling to the hot bath, the steady state of the system still contains information about T_c .

Conclusion.— In conclusion, we investigated the use of thermal machines as thermometers. The non-equilibrium nature of the steady state in these systems allows for simultaneously cooling the cold bath while determining its temperature. Furthermore, our scheme only requires the measurement of the power consumption and the hot temperature, both of which do not require any projective measurements on the quantum system which are difficult to implement. For realistic parameters, an implementation in circuit QED allows for precise thermometry ($\Delta T_c \lesssim 2$ mK) down to small temperatures ($T_c \sim 15$ mK). While slightly lower values have been

reported (see e.g. Ref. [22] where precise thermometry down to 6 mK has been reported) our scheme is of particular interest when heating of the sample has to be avoided and can be readily adapted to other architectures.

Acknowledgements.— PH, JB and NB acknowledge the Swiss National Science Foundation (Starting grant DIAQ and QSIT). MP acknowledges the Alexander von Humboldt Foundation, the CELLEX-ICFO-MPQ Research Fellowships, the Spanish MINECO (QIBEQI FIS2016-80773-P and SEV-2015-0522), and the Generalitat de Catalunya (SGR875 and CERCA).

-
- [1] L. D. Carlos and F. Palacio, eds., *Thermometry at the Nanoscale* (The Royal Society of Chemistry, 2016).
- [2] G. W. Walker, V. C. Sundar, C. M. Rudzinski, A. W. Wun, M. G. Bawendi, and D. G. Nocera, “Quantum-dot optical temperature probes,” *Appl. Phys. Lett.* **83**, 3555 (2003).
- [3] F. Seilmeier, M. Hauck, E. Schubert, G. J. Schinner, S. E. Beavan, and A. Högele, “Optical thermometry of an electron reservoir coupled to a single quantum dot in the millikelvin range,” *Phys. Rev. Applied* **2**, 024002 (2014).
- [4] F. Haupt, A. Imamoglu, and M. Kroner, “Single quantum dot as an optical thermometer for millikelvin temperatures,” *Phys. Rev. Applied* **2**, 024001 (2014).
- [5] D. M. Toyli, C. F. de las Casas, D. J. Christle, V. V. Dobrovitski, and D. D. Awschalom, “Fluorescence thermometry enhanced by the quantum coherence of single spins in diamond,” *Proc. Natl. Acad. Sci. U.S.A.* **110**, 8417 (2013).
- [6] G. Kucsko, P. C. Maurer, N. Y. Yao, M. Kubo, H. J. Noh, P. K. Lo, H. Park, and M. D. Lukin, “Nanometre-scale thermometry in a living cell,” *Nature* **500**, 54 (2013).
- [7] P. Neumann, I. Jakobi, F. Dolde, C. Burk, R. Reuter, G. Waldherr, J. Honert, T. Wolf, A. Brunner, J. H. Shim, D. Suter, H. Sumiya, J. Isoya, and J. Wrachtrup, “High-precision nanoscale temperature sensing using single defects in diamond,” *Nano Lett.* **13**, 2738 (2013).
- [8] D. Halbertal, J. Cuppens, M. Ben Shalom, L. Embon, N. Shadmi, Y. Anahory, H. R. Naren, J. Sarkar, A. Uri, Y. Ronen, Y. Myasoedov, L. S. Levitov, E. Joselevich, A. K. Geim, and E. Zeldov, “Nanoscale thermal imaging of dissipation in quantum systems,” *Nature* **539**, 407 (2016).
- [9] J. S. Donner, S. A. Thompson, M. P. Kreuzer, G. Baffou, and R. Quidant, “Mapping intracellular temperature using green fluorescent protein,” *Nano Lett.* **12**, 2107 (2012).
- [10] J. Goold, M. Huber, A. Riera, L. del Rio, and P. Skrzypczyk, “The role of quantum information in thermodynamics – a topical review,” *J. Phys. A: Math. Theor.* **49**, 143001 (2016).
- [11] S. Vinjanampathy and J. Anders, “Quantum thermodynamics,” *Contemp. Phys.* **57**, 545 (2016).
- [12] T. M. Stace, “Quantum limits of thermometry,” *Phys. Rev. A* **82**, 011611 (2010).
- [13] L. A. Correa, M. Mehboudi, G. Adesso, and A. Sanpera, “Individual quantum probes for optimal thermometry,” *Phys. Rev. Lett.* **114**, 220405 (2015).
- [14] A. De Pasquale, D. Rossini, R. Fazio, and V. Giovannetti, “Local quantum thermal susceptibility,” *Nat. Commun.* **7**, 12782 (2016).
- [15] S. Jevtic, D. Newman, T. Rudolph, and T. M. Stace, “Single-qubit thermometry,” *Phys. Rev. A* **91**, 012331 (2015).
- [16] T. H. Johnson, F. Cosco, M. T. Mitchison, D. Jaksch, and S. R. Clark, “Thermometry of ultracold atoms via nonequilibrium work distributions,” *Phys. Rev. A* **93**, 053619 (2016).
- [17] E. Martín-Martínez, A. Dragan, R. B. Mann, and I. Fuentes, “Berry phase quantum thermometer,” *New J. Phys.* **15**, 053036 (2013).
- [18] C. Sabín, A. White, L. Hackermuller, and I. Fuentes, “Impurities as a quantum thermometer for a Bose-Einstein condensate,” *Sci. Rep.* **4**, 6436 (2014).
- [19] L.-S. Guo, B.-M. Xu, J. Zou, and B. Shao, “Improved thermometry of low-temperature quantum systems by a ring-structure probe,” *Phys. Rev. A* **92**, 052112 (2015).
- [20] L. A. Correa, M. Perarnau-Llobet, K. V. Hovhannisyan, S. Hernández-Santana, M. Mehboudi, and A. Sanpera, “Low-temperature thermometry enhanced by strong coupling,” (2016), [arXiv:1611.10123 \[quant-ph\]](https://arxiv.org/abs/1611.10123).
- [21] F. Giazotto, T. T. Heikkilä, A. Luukanen, A. M. Savin, and J. P. Pekola, “Opportunities for mesoscopics in thermometry and refrigeration: Physics and applications,” *Rev. Mod. Phys.* **78**, 217 (2006).
- [22] Z. Iftikhar, A. Anthore, S. Jezouin, F. D. Parmentier, Y. Jin, A. Cavanna, A. Ouerghi, U. Gennser, and F. Pierre, “Primary thermometry triad at 6mK in mesoscopic circuits,” *Nat. Commun.* **7**, 12908 (2016).
- [23] R. Kosloff and A. Levy, “Quantum heat engines and refrigerators: Continuous devices,” *Annu. Rev. Phys. Chem.* **65**, 365 (2014).
- [24] H. T. Quan, Yu-xi Liu, C. P. Sun, and Franco Nori, “Quantum thermodynamic cycles and quantum heat engines,” *Phys. Rev. E* **76**, 031105 (2007).
- [25] N. Brunner, N. Linden, S. Popescu, and P. Skrzypczyk, “Virtual qubits, virtual temperatures, and the foundations of thermodynamics,” *Phys. Rev. E* **85**, 051117 (2012).
- [26] N. Linden, S. Popescu, and P. Skrzypczyk, “How small can thermal machines be? the smallest possible refrigerator,” *Phys. Rev. Lett.* **105**, 130401 (2010).
- [27] P. Skrzypczyk, N. Brunner, N. Linden, and S. Popescu,

- “The smallest refrigerators can reach maximal efficiency,” *J. Phys. A* **44**, 492002 (2011).
- [28] P. P. Hofer, M. Perarnau-Llobet, J. B. Brask, R. Silva, M. Huber, and N. Brunner, “Autonomous quantum refrigerator in a circuit QED architecture based on a Josephson junction,” *Phys. Rev. B* **94**, 235420 (2016).
- [29] M. T. Mitchison, M. Huber, J. Prior, M. P. Woods, and M. B. Plenio, “Realising a quantum absorption refrigerator with an atom-cavity system,” *Quantum Sci. Technol.* **1**, 015001 (2016).
- [30] A. Levy and R. Kosloff, “Quantum absorption refrigerator,” *Phys. Rev. Lett.* **108**, 070604 (2012).
- [31] M. T. Mitchison, M. P. Woods, J. P., and M. Huber, “Coherence-assisted single-shot cooling by quantum absorption refrigerators,” *New J. Phys.* **17**, 115013 (2015).
- [32] R. Silva, P. Skrzypczyk, and N. Brunner, “Small quantum absorption refrigerator with reversed couplings,” *Phys. Rev. E* **92**, 012136 (2015).
- [33] N. Brunner, M. Huber, N. Linden, S. Popescu, R. Silva, and P. Skrzypczyk, “Entanglement enhances cooling in microscopic quantum refrigerators,” *Phys. Rev. E* **89**, 032115 (2014).
- [34] J. B. Brask and N. Brunner, “Small quantum absorption refrigerator in the transient regime: Time scales, enhanced cooling, and entanglement,” *Phys. Rev. E* **92**, 062101 (2015).
- [35] A. Roulet, S. Nimmrichter, J. M. Arrazola, and V. Scarani, “Autonomous rotor heat engine,” (2016), [arXiv:1609.06011 \[quant-ph\]](https://arxiv.org/abs/1609.06011).
- [36] J. E. Geusic, E. O. Schulz-DuBois, and H. E. D. Scovil, “Quantum equivalent of the Carnot cycle,” *Phys. Rev.* **156**, 343 (1967).
- [37] See supplemental Material below for analytical results using a simplified model.
- [38] *Quantum Thermodynamics: Emergence of Thermodynamic Behavior Within Composite Quantum Systems*, Lecture Notes in Physics, Vol. 784 (Springer (Berlin), 2009).
- [39] R. Kosloff, “A quantum mechanical open system as a model of a heat engine,” *J. Chem. Phys.* **80**, 1625 (1984).
- [40] T. Feldmann and R. Kosloff, “Quantum four-stroke heat engine: Thermodynamic observables in a model with intrinsic friction,” *Phys. Rev. E* **68**, 016101 (2003).
- [41] A. O. Niskanen, Y. Nakamura, and J. P. Pekola, “Information entropic superconducting microcooler,” *Phys. Rev. B* **76**, 174523 (2007).
- [42] M. J. Henrich, F. Rempp, and G. Mahler, “Quantum thermodynamic Otto machines: A spin-system approach,” *Eur. Phys. J. ST* **151**, 157 (2007).
- [43] P. P. Hofer, J.-R. Souquet, and A. A. Clerk, “Quantum heat engine based on photon-assisted Cooper pair tunneling,” *Phys. Rev. B* **93**, 041418(R) (2016).
- [44] M. Campisi and R. Fazio, “The power of a critical heat engine,” *Nat. Commun.* **7**, 11895 (2016).
- [45] O.-P. Saira, M. Zgirski, K. L. Viisanen, D. S. Golubev, and J. P. Pekola, “Dispersive thermometry with a Josephson junction coupled to a resonator,” *Phys. Rev. Applied* **6**, 024005 (2016).
- [46] A. S. Holevo, *Probabilistic and Statistical Aspect of Quantum Theory* (North-Holland, Amsterdam, 1982).
- [47] S. L. Braunstein and C. M. Caves, “Statistical distance and the geometry of quantum states,” *Phys. Rev. Lett.* **72**, 3439 (1994).
- [48] A. Monras, “Phase space formalism for quantum estimation of Gaussian states,” [arXiv:1303.3682 \[quant-ph\]](https://arxiv.org/abs/1303.3682).
- [49] Zhang Jiang, “Quantum Fisher information for states in exponential form,” *Phys. Rev. A* **89**, 032128 (2014).
- [50] D. Šafránek and I. Fuentes, “Optimal probe states for the estimation of Gaussian unitary channels,” *Phys. Rev. A* **94**, 062313 (2016).
- [51] C. Sparaciari, S. Olivares, and M. G. A. Paris, “Gaussian-state interferometry with passive and active elements,” *Phys. Rev. A* **93**, 023810 (2016).

Supplement: Quantum Thermal Machine as a Thermometer

I. APPROXIMATE MODEL

Here we consider the approximate model that is obtained from the master equation in the main text by the replacement $(E_J/2)\hat{A}_c\hat{A}_h \rightarrow g$, leading to the Hamiltonian and current operator

$$\hat{H}_T = g \left(\hat{a}_h^\dagger \hat{a}_c + H.c. \right), \quad \hat{I}_T = i2eg \left(\hat{a}_c^\dagger \hat{a}_h - H.c. \right), \quad (\text{S1})$$

where g is treated as a fitting parameter. Such a model has first been investigated as a heat engine in Ref. [39]. An analogous engine that is based on coupled qubits instead of harmonic oscillators was introduced in Ref. [25]. The time-evolution of the harmonic oscillators is described by the local Lindblad master equation

$$\frac{\partial \hat{\rho}}{\partial t} = -i[\hat{H}_T, \hat{\rho}] + \kappa_h(n_B^h + 1)\mathcal{D}[\hat{a}_h]\hat{\rho} + \kappa_h n_B^h \mathcal{D}[\hat{a}_h^\dagger]\hat{\rho} + \kappa_c(n_B^c + 1)\mathcal{D}[\hat{a}_c]\hat{\rho} + \kappa_h n_B^c \mathcal{D}[\hat{a}_c^\dagger]\hat{\rho}, \quad (\text{S2})$$

with

$$\mathcal{D}[\hat{A}]\hat{\rho} = \hat{A}\hat{\rho}\hat{A}^\dagger - \frac{1}{2}\{\hat{A}^\dagger\hat{A}, \hat{\rho}\}, \quad (\text{S3})$$

and the Bose-Einstein distribution

$$n_B^\alpha = \frac{1}{e^{\frac{\Omega_\alpha}{k_B T_\alpha}} - 1}. \quad (\text{S4})$$

As usual, differential equations for averages of operators are obtained by

$$\partial_t \langle \hat{A} \rangle = \text{Tr}\{\hat{A}\partial_t \hat{\rho}\}. \quad (\text{S5})$$

Here we are interested in steady state values, where $\partial_t \langle \hat{A} \rangle = 0$. For the mean current, this yields

$$\langle \hat{I}_T \rangle = -2e \frac{4\kappa_h \kappa_c g^2 (n_B^h - n_B^c)}{(\kappa_h + \kappa_c)(\kappa_h \kappa_c + 4g^2)}, \quad (\text{S6})$$

which is plotted in Fig. 3 (a). The uncertainty in the temperature measurement plotted in Fig. 3 (b) is obtained using

$$\left(\frac{\partial f}{\partial P} \right)^2 (\Delta P)^2 = \left(\frac{\partial \langle \hat{I}_T \rangle}{\partial T_c} \right)^{-2} (\Delta I)^2, \quad (\text{S7})$$

and

$$\frac{\partial \langle \hat{I}_T \rangle}{\partial T_c} = \frac{2\kappa_h \kappa_c g^2}{(\kappa_h + \kappa_c)(\kappa_h \kappa_c + 4g^2)} \frac{e\Omega_c}{k_B T_c^2} \sinh^{-2} \left(\frac{\Omega_c}{2k_B T_c} \right), \quad (\text{S8})$$

which yields the error

$$\Delta T_c = \sqrt{\left[\frac{k_B T_c^2}{e\Omega_c} \sinh^2 \left(\frac{\Omega_c}{2k_B T_c} \right) \frac{(\kappa_h + \kappa_c)(\kappa_c \kappa_h + 4g^2)}{2\kappa_c \kappa_h g^2} \right]^2 (\Delta I)^2 + \left(\frac{\Omega_c}{\Omega_h} \right)^2 (\Delta T_h)^2}. \quad (\text{S9})$$

A. Steady-state solution

The steady state solution of the master equation in Eq. (S2) is Gaussian because the equation is bi-linear in creation and annihilation operators. It is therefore completely characterised by the first and second order moments of the quadrature operators

$$\hat{x}_\alpha = \frac{1}{\sqrt{2}}(\hat{a}_\alpha + \hat{a}_\alpha^\dagger), \quad \hat{p}_\alpha = \frac{1}{i\sqrt{2}}(\hat{a}_\alpha - \hat{a}_\alpha^\dagger). \quad (\text{S10})$$

Furthermore, since no term in the master equation induces displacements, the state is centred in phase space, $\langle \hat{x}_\alpha \rangle = \langle \hat{p}_\alpha \rangle = 0$, and is thus determined by the second moments alone.

We note that because the evolution is not unitary, it is not possible to determine the second moments simply by solving the equations of motions for the quadrature operators (working in the Heisenberg picture). While for unitary evolution, the time evolution of a product of operators is equal to the product of the time-evolved operators – e.g. $(\hat{x}_\alpha \hat{p}_\alpha)(t) = \hat{x}_\alpha(t) \hat{p}_\alpha(t)$ – this is not true in general. Hence, we need to derive the equations of motion for each of the second moments separately. We consider the 10 second moments $\langle \hat{x}_c^2 \rangle$, $\langle \hat{x}_c \hat{p}_c \rangle$, $\langle \hat{p}_c^2 \rangle$, $\langle \hat{x}_h^2 \rangle$, $\langle \hat{x}_h \hat{p}_h \rangle$, $\langle \hat{p}_h^2 \rangle$, $\langle \hat{x}_c \hat{x}_h \rangle$, $\langle \hat{x}_c \hat{p}_h \rangle$, $\langle \hat{p}_c \hat{x}_h \rangle$, $\langle \hat{p}_c \hat{p}_h \rangle$ (the remaining six are determined by the commutation relations). From (S2), we find

$$\begin{aligned}
\frac{\partial}{\partial t} \langle \hat{x}_c^2 \rangle &= 2g \langle \hat{x}_c \hat{p}_h \rangle - \kappa_c \langle \hat{x}_c^2 \rangle + \kappa_c (n_B^c + \frac{1}{2}), \\
\frac{\partial}{\partial t} \langle \hat{x}_c \hat{p}_c \rangle &= -g(\langle \hat{x}_c \hat{x}_h \rangle - \langle \hat{p}_c \hat{p}_h \rangle) - \kappa_c \hat{x}_c \hat{p}_c + \frac{i}{2} \kappa_c, \\
\frac{\partial}{\partial t} \langle \hat{p}_c^2 \rangle &= -2g \langle \hat{p}_c \hat{x}_h \rangle - \kappa_c \langle \hat{p}_c^2 \rangle + \kappa_c (n_B^c + \frac{1}{2}), \\
\frac{\partial}{\partial t} \langle \hat{x}_h^2 \rangle &= 2g \langle \hat{p}_c \hat{x}_h \rangle - \kappa_h \langle \hat{x}_h^2 \rangle + \kappa_h (n_B^h + \frac{1}{2}), \\
\frac{\partial}{\partial t} \langle \hat{x}_h \hat{p}_h \rangle &= -g(\langle \hat{x}_c \hat{x}_h \rangle - \langle \hat{p}_c \hat{p}_h \rangle) - \kappa_h \langle \hat{x}_h \hat{p}_h \rangle + \frac{i}{2} \kappa_h, \\
\frac{\partial}{\partial t} \langle \hat{p}_h^2 \rangle &= -2g \langle \hat{x}_c \hat{p}_h \rangle - \kappa_h \langle \hat{p}_h^2 \rangle + \kappa_h (n_B^h + \frac{1}{2}), \\
\frac{\partial}{\partial t} \langle \hat{x}_c \hat{x}_h \rangle &= g(\langle \hat{x}_c \hat{p}_c \rangle + \langle \hat{x}_h \hat{p}_h \rangle - i) - \frac{1}{2}(\kappa_c + \kappa_h) \langle \hat{x}_c \hat{x}_h \rangle, \\
\frac{\partial}{\partial t} \langle \hat{x}_c \hat{p}_h \rangle &= -g(\langle \hat{x}_c^2 \rangle - \langle \hat{p}_h^2 \rangle) - \frac{1}{2}(\kappa_c + \kappa_h) \langle \hat{x}_c \hat{p}_h \rangle, \\
\frac{\partial}{\partial t} \langle \hat{p}_c \hat{x}_h \rangle &= -g(\langle \hat{x}_h^2 \rangle - \langle \hat{p}_c^2 \rangle) - \frac{1}{2}(\kappa_c + \kappa_h) \langle \hat{p}_c \hat{x}_h \rangle, \\
\frac{\partial}{\partial t} \langle \hat{p}_c \hat{p}_h \rangle &= -g(\langle \hat{x}_c \hat{p}_c \rangle + \langle \hat{x}_h \hat{p}_h \rangle - i) - \frac{1}{2}(\kappa_c + \kappa_h) \langle \hat{p}_c \hat{p}_h \rangle.
\end{aligned} \tag{S11}$$

The steady state is found by setting all the derivatives to zero. We then get

$$\begin{aligned}
\langle \hat{x}_c^2 \rangle = \langle \hat{p}_c^2 \rangle &= \left(n_B^c + \frac{1}{2} \right) + \frac{g^2 \kappa_h}{(\kappa_c + \kappa_h)(g^2 + \kappa_c \kappa_h)} (n_B^h - n_B^c), \\
\langle \hat{x}_h^2 \rangle = \langle \hat{p}_h^2 \rangle &= \left(n_B^h + \frac{1}{2} \right) + \frac{g^2 \kappa_c}{(\kappa_c + \kappa_h)(g^2 + \kappa_c \kappa_h)} (n_B^c - n_B^h), \\
\langle \hat{x}_c \hat{p}_h \rangle = -\langle \hat{p}_c \hat{x}_h \rangle &= \frac{g \kappa_c \kappa_h}{(\kappa_c + \kappa_h)(g^2 + \kappa_c \kappa_h)} (n_B^h - n_B^c), \\
\langle \hat{x}_c \hat{p}_c \rangle = \langle \hat{x}_h \hat{p}_h \rangle &= \frac{i}{2}, \quad \langle \hat{x}_c \hat{x}_h \rangle = \langle \hat{p}_c \hat{p}_h \rangle = 0.
\end{aligned} \tag{S12}$$

We note that for $g = 0$ this is indeed a product of thermal states at temperatures T_c and T_h as expected. Also note that at the Carnot point we have $n_B^c = n_B^h$, which also results in a product of thermal states.

II. COMPUTING THE FISHER INFORMATION

From the first and second moments of the quadratures – i.e. from the covariance matrix, and the displacement vector (if the latter is non-zero) – it is possible to compute the QFI, with respect to a given parameter of interest (in our case this is the cold bath temperature T_c). Various works have considered this problem, e.g. [48–51]. Here, we will follow the method of [51].

We define a vector of the quadratures $\mathbf{r} = (\hat{x}_c, \hat{x}_h, \hat{p}_c, \hat{p}_h)$ (note that this ordering is not the same as in [51], nevertheless their method still applies, see also [49]). We restrict ourselves to the case where the first moments vanish, and define the covariance matrix as

$$\Gamma_{ij} = \frac{1}{2} \langle \hat{r}_i \hat{r}_j + \hat{r}_j \hat{r}_i \rangle. \tag{S13}$$

The canonical commutation relations are given by $[\hat{r}_i, \hat{r}_j] = i\Omega_{ij}$, where the symplectic matrix Ω with this ordering of the r_i is

$$\Omega = \begin{pmatrix} 0 & 0 & 1 & 0 \\ 0 & 0 & 0 & 1 \\ -1 & 0 & 0 & 0 \\ 0 & -1 & 0 & 0 \end{pmatrix}. \quad (\text{S14})$$

To compute the quantum Fisher information following [51], one needs to find a symplectic diagonalisation of the covariance matrix. That is, one needs to find a transformation S such that

$$S\Omega S^T = \Omega, \quad (\text{S15})$$

and

$$S\Gamma S^T = \Gamma_S, \quad (\text{S16})$$

where Γ_S is diagonal. One can then proceed to define the matrix Φ_S by

$$(\Phi_S)_{ij} = \frac{(\Omega^T \Gamma_S \dot{\Gamma}_S \Gamma_S \Omega + \frac{1}{4} \dot{\Gamma}_S)_{ij}}{2\lambda_i^2 \lambda_j^2 - \frac{1}{8}}, \quad (\text{S17})$$

where the dot denotes derivation with respect to T_c , and λ_α are the eigenvalues of Γ . One further defines $\Phi = S^{-1} \Phi_S (S^T)^{-1}$, and the QFI is finally given by

$$F_{T_c} = \text{Tr}[\Omega^T \dot{\Gamma} \Omega \Phi]. \quad (\text{S18})$$

The symplectic diagonalisation is the most involved step of computing the QFI. For the steady-state solution in Eqs. (S12)

$$\Gamma = \begin{pmatrix} a & 0 & 0 & -c \\ 0 & b & c & 0 \\ 0 & c & a & 0 \\ -c & 0 & 0 & b \end{pmatrix}, \quad (\text{S19})$$

where

$$a = \frac{1}{2}(1 + 2n_B^c - \nu\kappa_c), \quad b = \frac{1}{2}(1 + 2n_B^h + \nu\kappa_h), \quad c = \frac{1}{4g}\kappa_c\kappa_h\nu, \quad (\text{S20})$$

and

$$\nu = \frac{8g^2(n_B^c - n_B^h)}{(\kappa_c + \kappa_h)(4g^2 + \kappa_c\kappa_h)}. \quad (\text{S21})$$

Denoting the normalized eigenvectors of Γ as row vectors by v_i , $i = 1, 2, 3, 4$, a symplectic transformation diagonalizing Γ can be constructed as

$$S = \begin{pmatrix} \text{Im}(v_1) \\ \text{Im}(v_3) \\ \text{Re}(v_1) \\ \text{Re}(v_3) \end{pmatrix}, \quad (\text{S22})$$

where Re and Im denote real and imaginary parts respectively. One finds that

$$\Gamma_S = S\Gamma S^T = \begin{pmatrix} a' & 0 & 0 & 0 \\ 0 & b' & 0 & 0 \\ 0 & 0 & a' & 0 \\ 0 & 0 & 0 & b' \end{pmatrix}, \quad (\text{S23})$$

with

$$a' = \frac{1}{2} \left(a + b + \sqrt{(a-b)^2 + 4c^2} \right), \quad b' = \frac{1}{2} \left(a + b - \sqrt{(a-b)^2 + 4c^2} \right). \quad (\text{S24})$$

From Eqs. (S17) and (S18), and by using that close to the Carnot point

$$n_B^c - n_B^h = \frac{1}{e^{\Omega_c/T_c} - 1} - \frac{1}{e^{\Omega_c/T_c + \epsilon} - 1} \approx n_B^c (n_B^c + 1) \epsilon, \quad (\text{S25})$$

the expression for the QFI at the Carnot point can be found by taking the limit $\epsilon \rightarrow 0$ and reads

$$F_{T_c} = \frac{\kappa_c^2 (8g^2 \kappa_h (\kappa_c + 2\kappa_h) + \kappa_h^2 (\kappa_c + \kappa_h)^2 + 32g^4) \Omega_c^2}{4 (\kappa_c + \kappa_h)^2 (\kappa_c \kappa_h + 4g^2)^2} \frac{1}{T_c^4 \sinh^2(\Omega_c/2T_c)}. \quad (\text{S26})$$

The parameter β in the main text thus reads

$$\beta = \frac{2 (\kappa_c + \kappa_h) (\kappa_c \kappa_h + 4g^2)}{\kappa_c \sqrt{8g^2 \kappa_c \kappa_h + \kappa_h^2 (\kappa_c^2 + 16g^2) + 2\kappa_c \kappa_h^3 + 32g^4 + \kappa_h^4}}. \quad (\text{S27})$$

III. COMPUTING THE UNCERTAINTY FROM A CURRENT MEASUREMENT

We aim to use Eq. (12) for the simple model given in Eq. (S1) in the steady state. The mean current $\langle \hat{I}_T \rangle$ and its derivative with respect to T_c are given in Eqs. (S6) and (S8) respectively. The variance $(\Delta \hat{I}_T)^2 = \langle \hat{I}_T^2 \rangle - \langle \hat{I}_T \rangle^2$ reads

$$\begin{aligned} (\Delta \hat{I}_T)^2 = (2e)^2 g^2 & \left(n_B^c (n_B^h + 1) + n_B^h (n_B^c + 1) + \frac{8g^2 (n_B^h - n_B^c)}{(\kappa_h + \kappa_c)(\kappa_h \kappa_c + 4g^2)} [\kappa_h (n_B^h + 1/2) - \kappa_c (n_B^c + 1/2)] \right. \\ & \left. - \frac{32g^4 \kappa_h \kappa_c (n_B^h - n_B^c)^2}{(\kappa_h + \kappa_c)^2 (\kappa_h \kappa_c + 4g^2)^2} \right), \end{aligned} \quad (\text{S28})$$

which simplifies to

$$(\Delta \hat{I}_T)^2 = 2(2e)^2 g^2 n_B^c (n_B^c + 1) = 2e^2 g^2 \frac{1}{\sinh^2(\Omega_c/2T_c)}, \quad (\text{S29})$$

at the Carnot point where we have $n_B^c = n_B^h$. Hence, we get that with a current measurement at the Carnot point

$$(\Delta T_c)_I^2 = \frac{(\kappa_h + \kappa_c)^2 (\kappa_h \kappa_c + 4g^2)^2 T_c^4}{2\kappa_h^2 \kappa_c^2 g^2} \frac{1}{\Omega_c^2} \sinh^2(\Omega_c/2T_c), \quad (\text{S30})$$

which results in

$$\alpha = \frac{(\kappa_h + \kappa_c)(\kappa_h \kappa_c + 4g^2)}{\sqrt{2\kappa_h \kappa_c} g}. \quad (\text{S31})$$